PROCEEDINGS, 50th Workshop on Geothermal Reservoir Engineering
Stanford University, Stanford, California, February 10-12, 2025
SGP-TR-229

Structural, Mineralogical, and Geophysical Data Implications for the Development of the Salton Sea Magma-Hydrothermal System

Danny B. Sims[1], Philip S. Neuhoff[2] and Denis L. Norton[3]

[1]CTR, 124 W. 9th St. Suite 101, Imperial, CA 92251 [2]Consulting Geologist, Eagle, Idaho [3]School of Thought, Stanley, Idaho

Danny.sims@cthermal.com

Keywords: Salton Sea Geothermal Field, mineralogy, structural geology, geophysics, permeability, lithium, reservoir model

ABSTRACT

Structural, mineralogical and seismic reflection data from Controlled Thermal Resources (CTR) Hell's Kitchen Project, and mineralogical and seismic reflection data from the EnergySource Minerals/Cyrq Energy Hudson Ranch Project, are incorporated into a geological model describing the dynamic Salton Sea magma-hydrothermal system. The resulting model predicts natural flow paths that extend to much greater depth than previously published numerical reservoir models, allowing better estimation of mineralized brine sourceregions, the fate of injected mineral-depleted brine, and Li depletion rates.

Within this transtensional-dilational stepover basin, strain is accommodated by presently forming NNE striking structures and reactivation of earlier-formed NE and NW striking faults, accompanied by magma intrusions, thermally driven hydrofractures and seismicity, and development of the youthful oblique slip Brawley Fault. This system is well-described as a Hill-type mesh, with magmatism, high thermal gradients, high fluid pressures, and brine upflow centers coincident with stepovers. Temperature and mineralogical data obtained from XRD analysis demonstrate the dynamic nature of the thermal regime. Changes in mineral assemblages and mineral abundance with depth reflect the location of the high salinity brine dominating the reservoir, the temporal progradation of temperature, and zones of enhanced advective fluid transport.

1. INTRODUCTION

The Salton Sea Geothermal Field (SSGF) in southern California, USA, hosts 437 MW of installed capacity and prior reservoir modelling work at the SSGF focused on the production of geothermal power. Geothermal brines in the SSGF contain Li and other metals that are increasingly the subject of exploration and development efforts. Published static and numerical reservoir models for SSGF Li potential are limited to about 500 feet below the deepest wells (approximately 3 km depth), but within this magma-hydrothermal system, predicted flow paths extend down to a depth below the recorded earthquakes (approximately 10 km). A comprehensive geologic model is necessary to provide a basis for realistic reservoir engineering-derived mineral depletion forecasts. This paper outlines the geologic interpretations necessary for such a model, leveraging observations resulting from recent drilling at the CTR Hell's Kitchen Project and prior work at the nearby Hudson Ranch Project[1].

2. WELL DATA

CTR drilled two production wells. Well P1-1 was drilled at 308° azimuth. The total measured depth is 8,000 feet and the total vertical depth is 6,734 feet. Well P1-2 was drilled at 197° azimuth. The total measured depth is 8,618 feet and the total vertical depth is 8,056 feet. All downhole depths reported herein are measured depth (MD). The initial capacities estimated from flow tests for the wells are 28 and 30 MW respectively (GeothermEx, 2022).

Cutting samples were collected on nominal 10-foot intervals. Mineralogy for samples from the wells was determined using a benchtop Rigaku Miniflex XRD. Structure and bedding orientation and density data were obtained using the Halliburton X-tended Range Micro Imager (XMRI^{TM}) wireline borehole imaging tool. The fracture and bedding data presented here were produced by Halliburton using the auto-pick function. Structure data are presented in lower hemisphere Schmidt plots. A 10° blind zone, where structures have a low probability of being intercepted because they nearly parallel the well (Terzaghi, 1965; Celwik et al., 2011), is plotted for each well.

Baker Hughes used well data to interpret that the maximum principal stress (σ_1) is near vertical, and the intermediate principal stress (σ_2) and maximum horizontal stress (S_{Hmax}) are nearly horizontal striking approximately 010°. This is similar to the interpretation of Crandall-Bear et al. (2018) for the stress field interpreted from well data and focal mechanisms in the central part of the SSGF.

2.1 Structure Convention

A geologic structure set comprises all faults and fractures within a structural domain that share a common orientation (strike and dip). There is a negative exponential or Weibel distribution for length and spacing of all structures within a set (Call et al., 1976; Nicholas and Sims, 2000). The longest structures are regional structures, and these are named faults that are identified on field-scale maps

[1] The authors previously presented Hudson Ranch data contained herein at California State University, San Marcos (Sims, 2013). Figures are reprinted with the generous permission of EnergySource Minerals and Cyrq Energy.

(Nicholas and Sims, 2000; Sims, 2017). A reasonable minimum cutoff limit for regional structure strike length at the SSGF is one mile. Structures with strike lengths below the cutoff limit comprise the rock fabric. Fault damage zones comprise fabric that is somewhat random in orientation (Evans et al., 1997) because of stress perturbations proximal to a fault, and the width of these zones is proportional to the distance of fault displacement (Faulkner et al., 2011). We refer to the rock volume outside regional fault damage zones, and containing fabric scale structures, as the rock mass.

Within the Imperial Valley there are three orientations for regional faults and their corresponding structure sets. (1) Regional structures that parallel the rift basin, including the San Andreas, Imperial, San Jacinto, Calipatria, and other faults, and fabric scale structures of the same orientation, are referred to in this paper as NW striking structures. (2) Regional faults that strike approximately perpendicular to the rift axis, including the Elmore Ranch, Kalin, Main Central, and other faults, and fabric scale structures of the same orientation, are referred to as NE striking structures. (3) Regional faults striking approximately N10E in the direction of S_{Hmax} and σ_2 include unnamed faults under the Salton Sea identified by Brothers et al. (2009) and others. These regional faults and fabric scale structures of the same orientation are referred to as NNE striking structures. The Brawley Fault Zone comprises a master linkage fault at depth and peak or post peak stage shear zone structures (Tchelanko, 1970) in the overlying sedimentary rock. These structures are unique within the SSGF system and the elements of this Reidel shear zone are not included as part of a structure set.

2.2 CTR Production Well P1-1

The drill path of production well P1-1 does not intercept a regional fault (Figure 1). A significant fluid loss zone was intersected at 5,630 feet. Epidote and authigenic K-feldspar abundance, which are indicative of a permeable zone in a well (Hulen et al., 2003), increased immediately below the fluid loss zone. Combining all data, Holt (2022) estimated that the P1-1 major feed zone is between 5,630 ft. and 6,020 ft.

Almost all structures recorded for well P1-1, including those within the major feed zone, are NNE striking structures with dips ranging from vertical to 60° (Figure 2). The average apparent fracture spacing for all logged fracture types between 3,882 and 7,969 ft. is 1.2 fractures/ft. To a measured depth of 6,815 ft., bedding is consistent with a dip of approximately 18° and dip direction of 220°. Below this depth, the orientation is consistently 20° dip and dip direction 175°.

Significant permeability zones are present below the production feed zone. At 7,690 ft. the lithology abruptly changed from siltstone and mudstone dominated rock above to sandstone dominated rock below. Faults and fractures are predominantly NNE striking with an east dip greater than 70°. NW striking structure is present but much less abundant. The well lost 360 barrels/hour (BPH) at the contact and continued losing 40-120 BPH to the bottom of the well. Euhedral epidote crystals that require porosity for growth, and whose length provide evidence for minimum aperture in open structures or pore spaces, were common in the bottom of the well.

2.3 CTR Production Well P1-2

The drill path of production well P1-2 lies within the same block of surrounding regional faults as well P1-1, but it penetrates the damage zone of the NW striking Estelle Fault (Figure 1). Holt (2022) provided that potential feed zones are between 5,100 ft and 7,800 feet. There was a total loss of returns between 4,060 and 4,152 feet. There is no image log for this interval, and it was behind casing for flow tests. Within the open hole, an abundance of alteration minerals commonly associated with flow zones (epidote, K-feldspar) is centered at about 5,350 feet measured depth. This depth coincides with a significant sharp and narrow temperature reversal zone in logs that were run during heat-up (Figure 3). This is commonly interpreted to result from cold mud infiltration during drilling, but no mud losses were recorded for the zone.

Relative to well P1-1, bedding is chaotic with an average orientation of approximately 10° dip and 250° dip direction. NNE striking structures are the most common and NW striking structures are much more abundant than in well P1-1. NE striking structures are the least abundant. There is a population of structures with dip angles lower than 60 degrees and strike directions that are variable (Figure 2). Apparent fracture frequency ranges from 0-2.5 fractures/ft., but the well is partially in the blind zone for NNE striking structure so that prolific set is poorly sampled.

At 7,700 ft. the lithology abruptly changed from siltstone and mudstone dominated rock above to sandstone dominated rock below. The well lost 70 BPH at the contact. At 7,920 feet the well began to lose 700 BPH associated with abundant alteration minerals and a drill break at 7,950 feet. The well lost between 140 and 700 BPH to the base of the sand dominated zone at 8,250 feet. Mud losses were between 18 and 120 BPH to the bottom of the well at 8,620 feet.

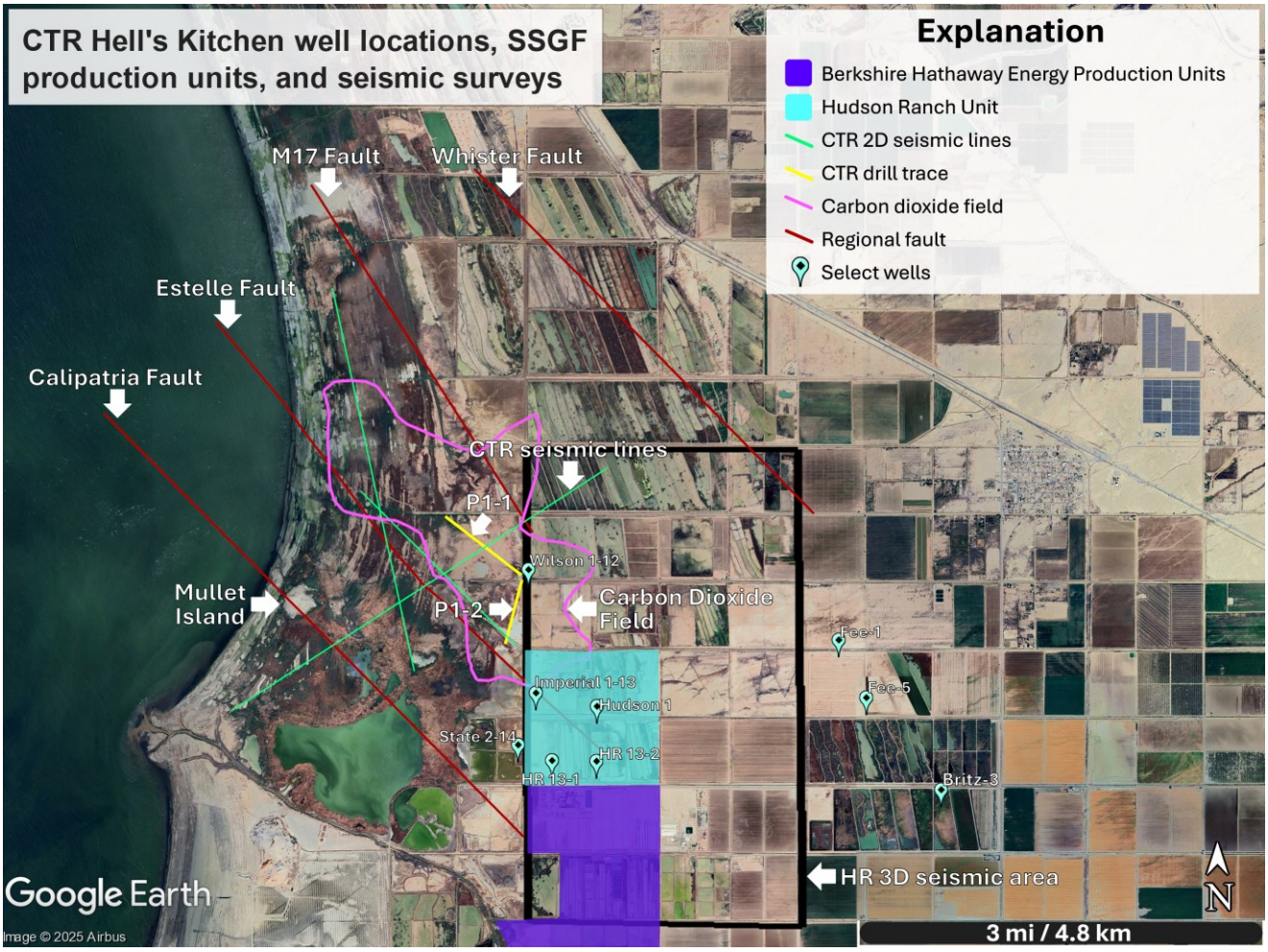

Figure 1: Southeast SSGF, geothermal production units, CTR well drill traces (yellow), select regional faults, select wellhead locations, seismic survey locations, and carbon dioxide field limit from well locations (USGS, 1944 and 1956). HR=Hudson Ranch, Hudson is a legacy well that predates HR development. The Calipatria Fault location shown is that described by Lynch and Hudnut (2008) who attribute its identification to earlier workers. We differ with more recent work that has moved the Calipatria Fault to a new location to the east and considers it to be the eastern edge of the field (e.g. Kaspereit et al., 2016).

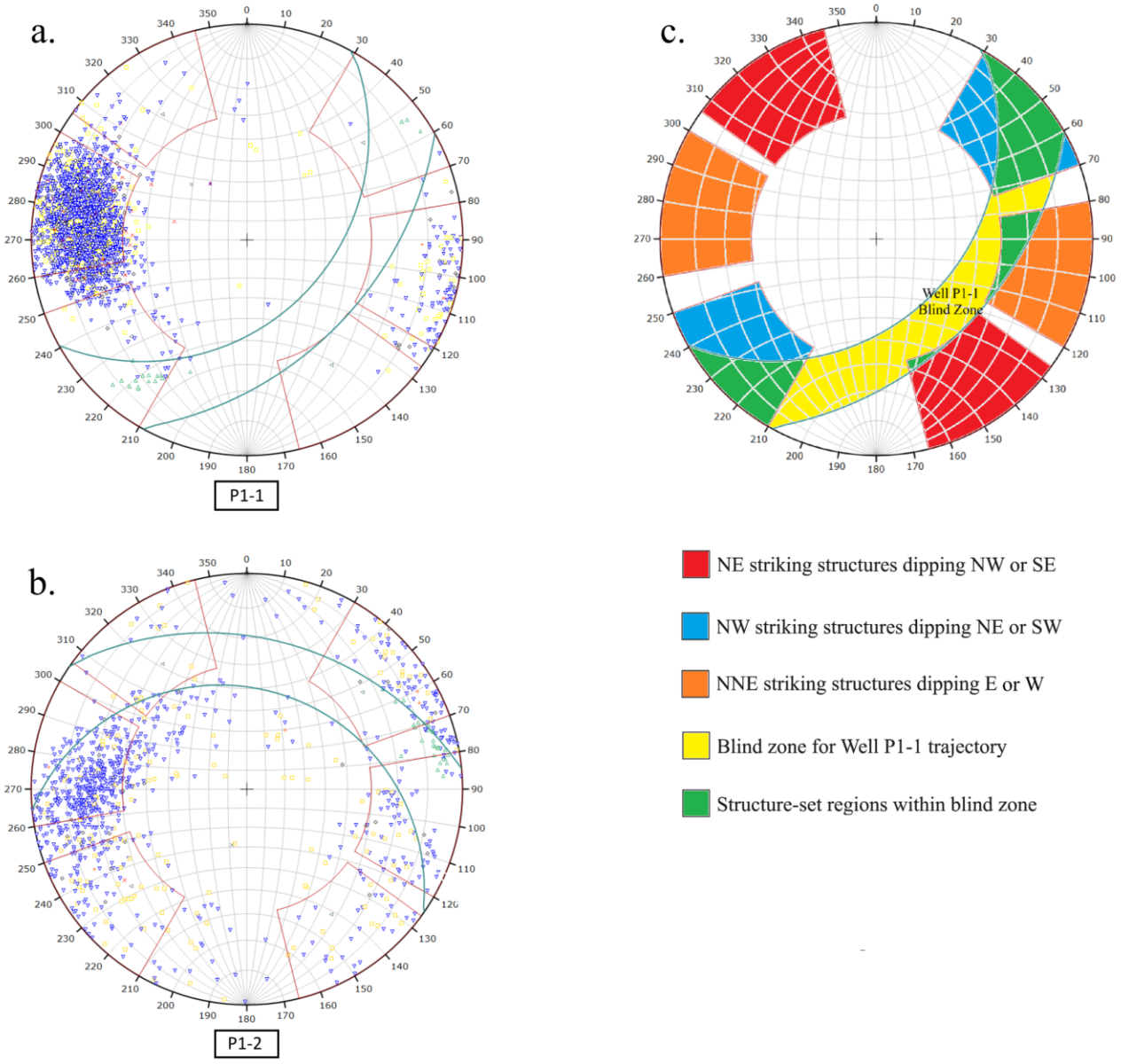

Figure 2: Structure data for CTR wells P1-1 and P1-2 on lower hemisphere Schmidt plots. The blind zone is between the two green great circles on each plot. A blue rectangle is a partial conductive fracture, a black diamond is a conductive fracture, a yellow square is a partial resistive fracture, a red x is a resistive fracture, and a green diamond is an induced fracture. (a.) All structures recorded in well P1-1. (b.) All structures recorded in well P1-2. (c.) Pole locations identified for Imperial Valley structure set orientations and the CTR well P1-1 blind zone.

2.4 Mineralogic Implications for the Dynamic Prograde Magma-Hydrothermal System

The static temperature profiles for both CTR wells fit squarely within the limits for Boundary Region profiles of Williams (1997) (Figure 3). The wells are within the 200°C/km contour on the shallow thermal gradient map of Newmark et al. (1988) and updated by Hulen et al. (2002). The authors performed XRD analysis for approximately 8,000 cuttings samples from CTR wells, Hudson Ranch wells and surrounding wells for which Dr. Wilfred Elders contributed cuttings (State 2-14, Wilson 1-12, Hudson, Imperial 1-13, and several Fee and Britz wells). Our interpretation that the system is thermally and metasomatically prograde is consistent with prior studies (e.g. Muffler and White, 1969; Tewhey, 1977; Muramoto and Elders, 1984; McDowell, 1987; Cho et al., 1988).

The dual porosity reservoir (open structures and sediment pore space), with brine temperature exceeding 500°F (260 ºC) and brine salinity exceeding 20%, is bound between the top of the albite zone, at a depth of approximately 4,500 feet in the CTR wells, and the top of the clinopyroxene zone at a depth of approximately 10,000 feet and a corresponding temperature of 660 °F (349 ºC) in well State

2-14 (Cho et al., 1988). Because wells are cooled while drilling, and metasomatism is prograde, XRD analysis performed at the drill pad at nominal 10-foot intervals is the best available tool for determining reservoir temperature and making critical decisions while drilling.

Evidence for the dynamic, prograde nature of the hydrothermal system in the vicinity of the CTR wells is provided by the relationship of measured temperature and depth distribution of minerals participating in the chlorite isograd reaction that marks the first appearance of chlorite:

$$5\ CaMg(CO_3)_2 + SiO_2 + Al_2Si_2O_5(OH)_4 + 2\ H_2O = Mg_5Al_2Si_3O_{10}(OH)_8 + 5\ CaCO_3 + 5\ CO_2$$

Dolomite Quartz Kaolinite Chlorite Calcite

In the Boundary Region of Williams (1997), this reaction occurs as a discrete change in mineralogy with kaolinite and dolomite disappearing abruptly at the depth where chlorite becomes part of the mineral assemblage (example from a Hudson Ranch well in Figure 4). Dolomite, kaolinite, and chlorite coexist in these wells only over a few hundred feet at most. In contrast, within the Distal Region of Williams (1997) kaolinite and dolomite persist below the chlorite isograd for as much as 2,500 feet, indicative of the active and incomplete reaction as the system progrades in this region. This behavior is observed in the Fee and Britz wells (Figure 1), where the geothermal gradient is relatively low, fluid inclusions indicate thermal equilibrium for select minerals (Chou, 1989), and high salinity brine (25% TDS) flowed from wells Fee#1 and #5 (Nielson and Moore, 1984). In well Fee #5, chlorite was first detected at 2,952 ft. and was abundant at a depth of 4,800 ft., which is the same depth that kaolinite became absent (Chou, 1989).

In CTR well P1-1, the static temperature profile is consistent for the Boundary Region (Figure 3). However, chlorite first appears at 900 feet MD and TVD, which is shallow for this part of field, and dolomite persists to 3,400 feet MD (3,220 TVD), which is very deep for this part of the field. We interpret the broad overlap zone within an area of Boundary Region temperature to result from a recent magma intrusion between the Estelle and M17 faults (Figure 1). The large volume of rock rapidly undergoing the dolomite-chlorite reaction (Figure 5) creates abundant carbon dioxide and this is the origin of the carbon dioxide field that the CTR wells are within (Figure 1). The carbon dioxide wells produced from sand zones at 400-600 ft. depth at 200-300 psi (Kelley and Soske, 1936; Fitch, 1961).

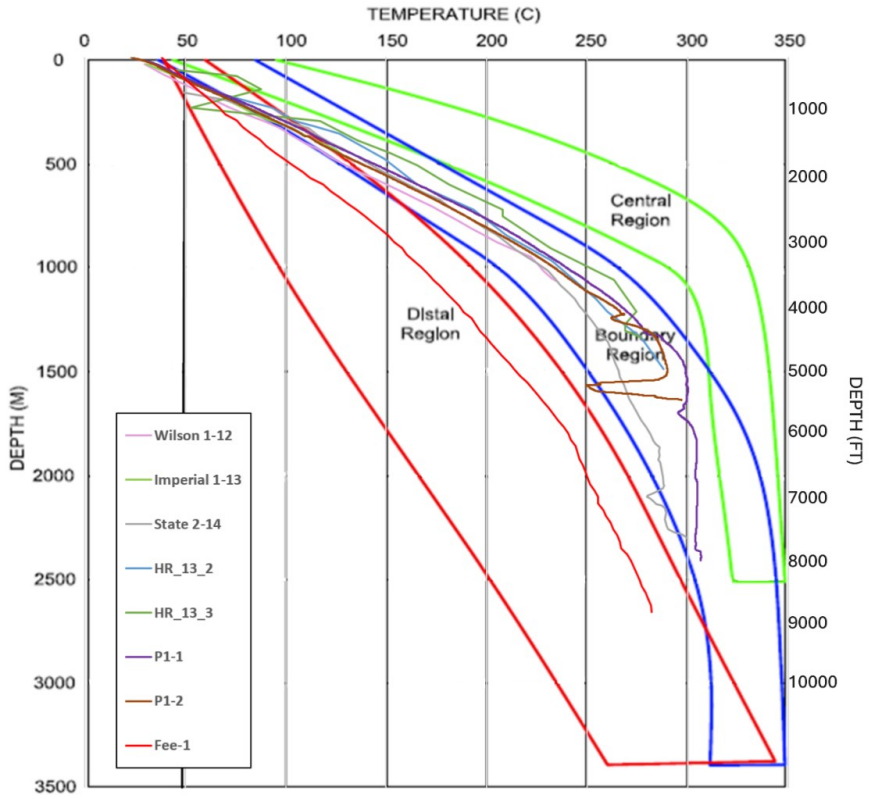

Figure 3: Temperature profiles for CTR wells, Hudson Ranch (HR) wells (CalGEM, 2025) and some of the select wells identified in Figure 1. Thermal profile limits for the Central (green), Boundary (blue) and Distal (red) Regions from Williams (1997).

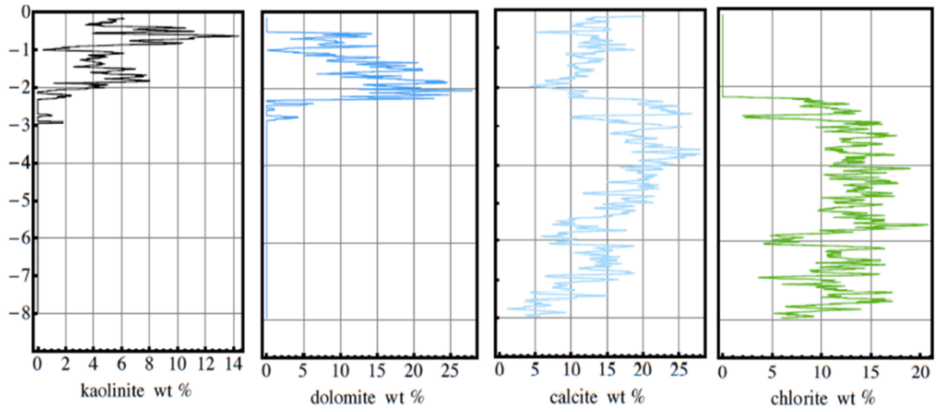

Figure 4: Mineral abundances for phases participating in the chlorite isograd reaction (see text) determined through quantitative XRD analysis of ~800 samples from a Hudson Ranch well (Sims, 2013). Vertical axis is MD in 1,000's of feet.

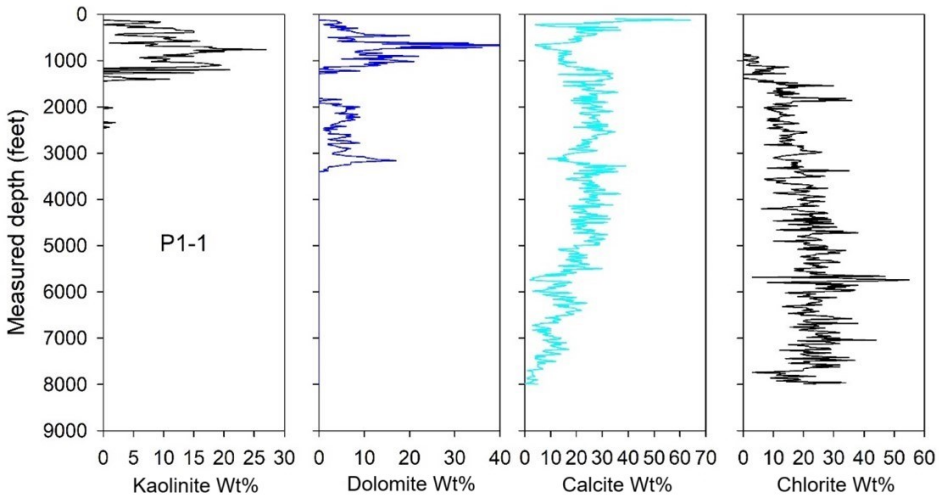

Figure 5: Mineral abundances for phases participating in the chlorite isograd reaction (see text) determined through quantitative XRD analysis of ~400 samples from CTR well P1-1.

3. SEISMIC REFLECTION

Seismic reflection is the best available technology for identifying discrete permeability targets in the Salton Trough. The method has been successfully used at Heber (James et al., 1987), East Mesa (Howard et al., 1978), the Hudson Ranch Unit at the SSGF (Sims, 2013), and at Cerro Prieto, Mexico (Blakeslee, 1984).

The Hudson Ranch 3D seismic survey identified an uppermost zone of continuous reflectors that dominate above the chlorite-calcite mineralogical zone. Within this same zone, CTR 2D seismic lines contain washed out, but continuous reflectors within drill-defined sand units and these are attributed to carbon dioxide gas in the formation. Brothers et al. (2009) reported similar results and conclusions for shallow seismic data offshore.

Production zones are within a deeper Poor Reflector Zone (PRZ) that differs from reflectors described above in that reflectors are washed out, discontinuous over short distances and somewhat randomly oriented (Figure 6). The PRZ is discordant to bedding and it does not relate to any primary lithology (Howard et al., 1978; James et al., 1987; Sims, 2013). The base of the PRZ is identified by a sharp transition to continuous reflectors of the Deep Prominent Reflectors Zone ("DPRZ"). This is coincident with the transition from greenschist to amphibolite grade metasomatic rock. It is also the base of the dual porosity reservoir, and it coincides with the 5.6 km/s seismic velocity surface mapped throughout the basin by Fuis and Kohler (1984) as the basement. For modelling, the Fuis and Kohler 5.6 km/s seismic velocity surface is field-wide depth corrected by the authors with a 0.25 km downward shift by incorporating data from Sims (2013) and Han (2016).

The shallow continuous reflectors, PRZ and DPRZ are shown in Hudson Ranch 3D seismic reflection lines in Figure 6. Crossline 269 is a 3.5-mile-long north-south line with north to the left. The bright reflectors in the center were not drill tested but are believed to be an intrusion. South of the intersection of Inline 224, the PRZ extends to within about 500 feet of the surface. The PRZ and DPRZ contacts were identified at every 660 ft. spaced crossline and inline intersection and used to create a 3D volume for the PRZ (Figure 7).

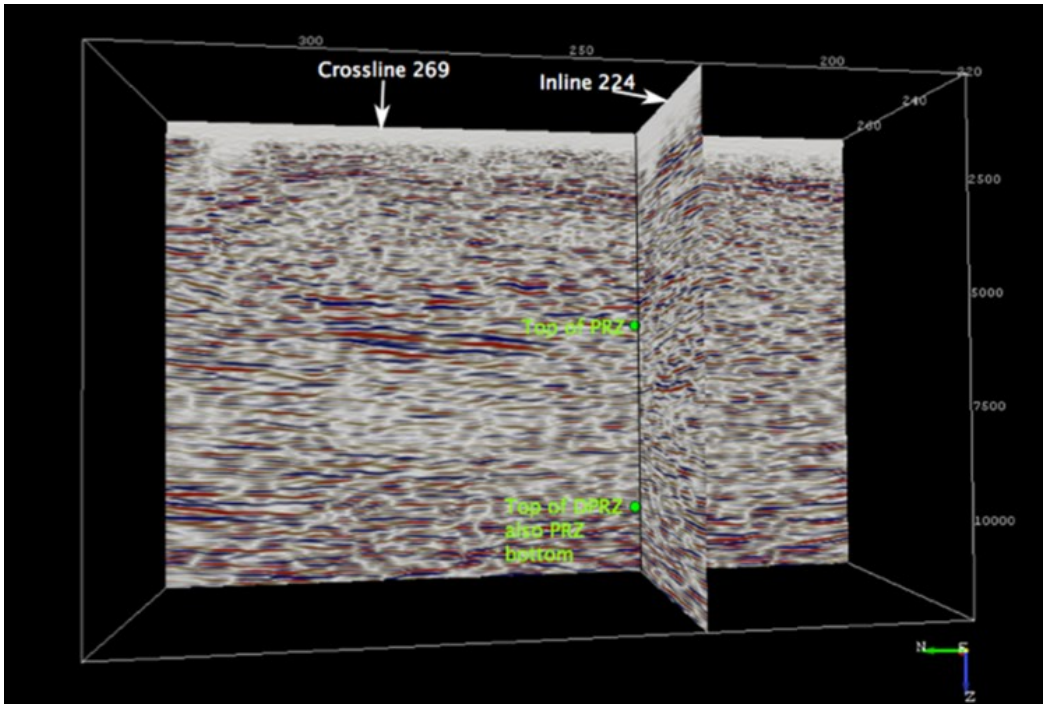

Figure 6: Hudson Ranch 3D seismic survey and PRZ and DPRZ surfaces. Depth is labeled in feet and the maximum depth for the seismic survey is 12,000 feet (Sims, 2013). The map location for the survey is indicated in Figure 1.

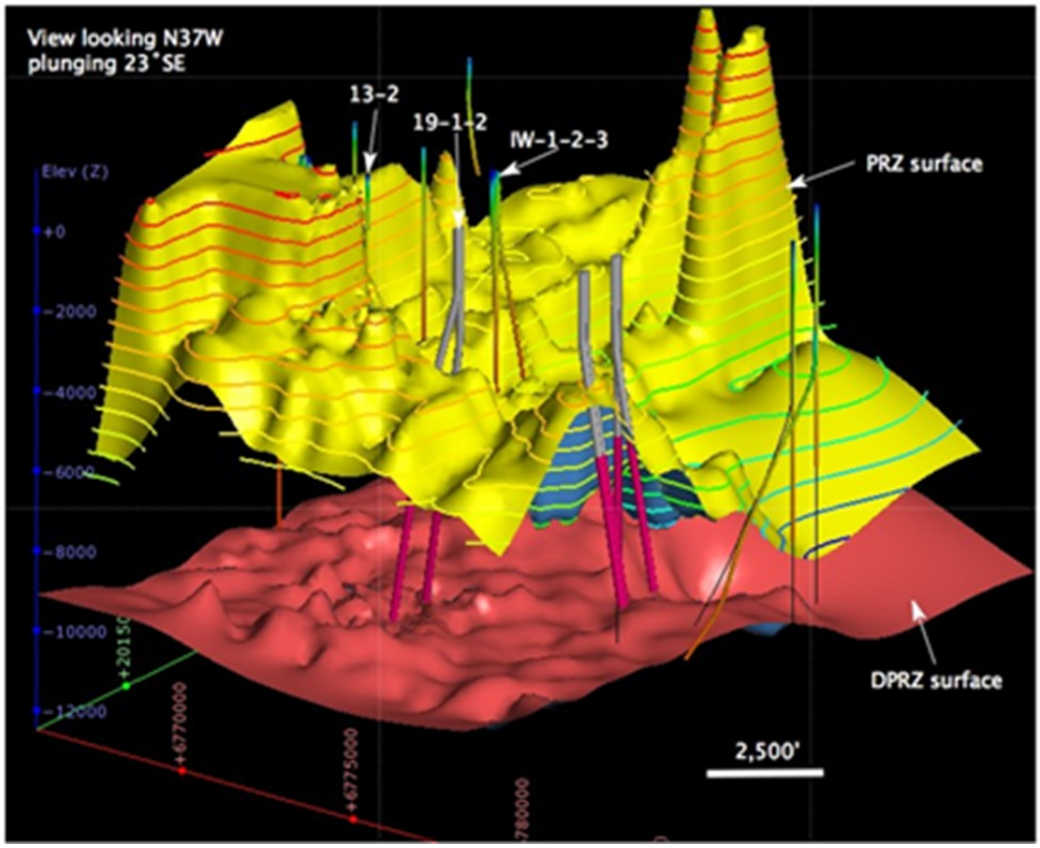

Figure 7: Hudson Ranch modelled PRZ and DPRZ surfaces. Depth is labeled in feet (Sims, 2013).

4. REGIONAL FAULTS

Except for the herein described Jacumba Lineament, the area of investigation is restricted to the region of sedimentary basin fill bound between crystalline basement outcrops of the North American and Pacific plates on the map of Fuis et al. (1982). The CTR model includes only regional faults that are verified by alignment of volcanic or thermal features at the surface, geophysical methods (see endnotes in Elders et al., 1972), well data, surface rupture, or earthquake data (Hauksson et al., 2012) (Figure 8).

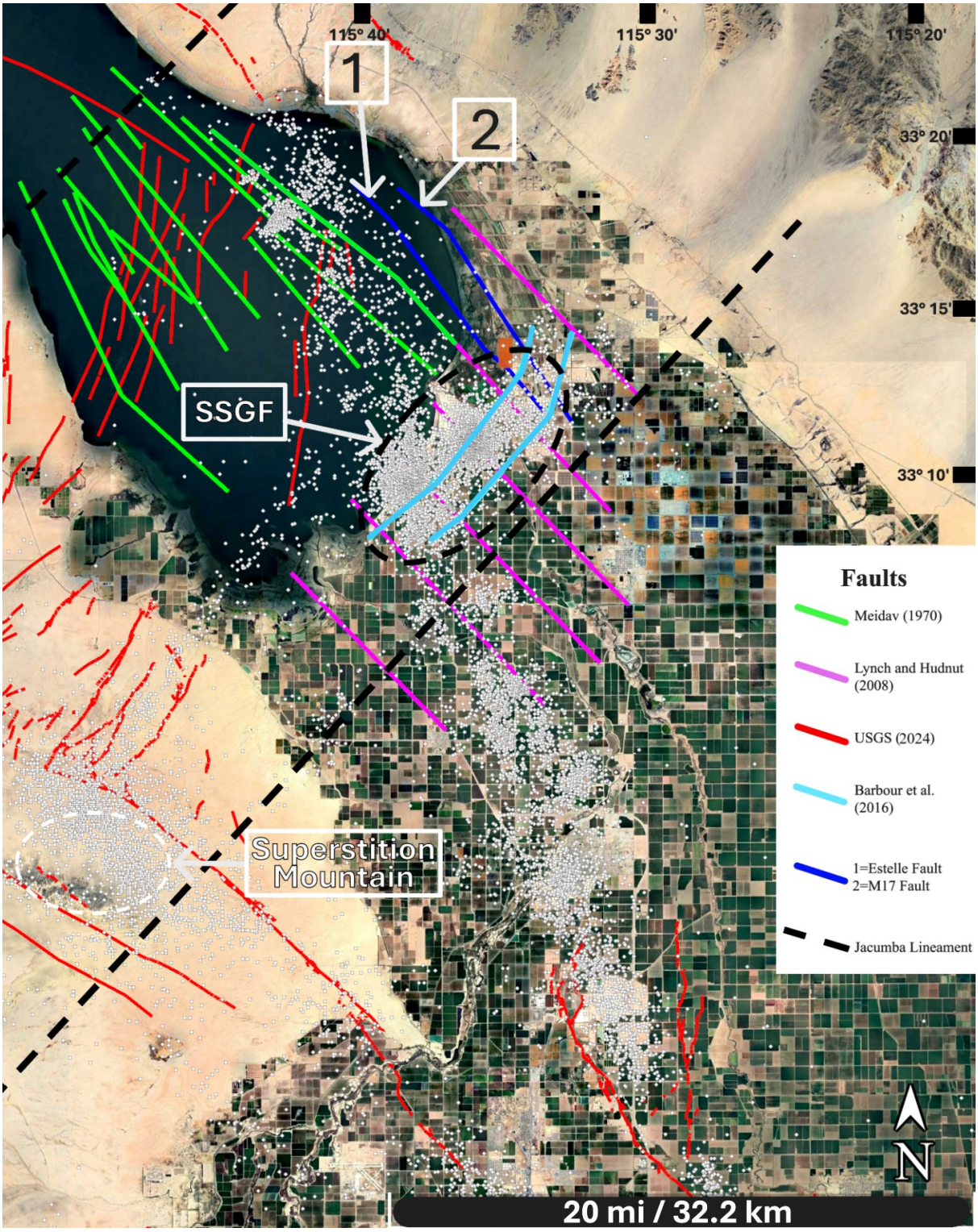

Figure 8: Modeled regional faults. Earthquakes (white dots) from USGS (2025). The brown rectangle between the Estelle and M17 faults is the CTR well locations.

4.1 NW Striking Regional Faults

NW striking regional faults parallel the Salton Trough and separate the Pacific Plate and North American Plate which are moving with right lateral relative displacement. These are residual stage Principal Displacement Zone (PDZ) faults as described by Tchelanko (1970). Earlier formed peak and post peak stage structures including Reidel shears (R), P shears (P), and conjugate Reidel shears (R') are not formed in the residual stage.

NW striking regional faults presented herein are taken or modified from Meidav (1970) and are those compiled by Lynch and Hudnut (2008). Meidav (1970) surveyed the southern half of the Salton Sea with five seismic lines approximately perpendicular to the axis of the basin. All faults belong to the NW striking set and they are identified by numbers. Relative offset and bedding orientation are indicated where known and a graben is indicated between the Estelle Fault and the Calipatria Fault.

The Calipatria Fault is the best described NW striking fault within the SSGF and it is the most significant permeability structure in the CTR Project area. Thermal features along the fault include the Mullet Island volcano, the center of an inferred shallow intrusion interpreted from a magnetic survey (Kelley and Soske, 1936), and a lineament of fumaroles. Sahakian et al. (2016) identified the NW striking Salton Trough Fault from seismic reflection and this is the north extension of Meidav's (1970) offshore Fault 14, and the onshore extension is the Calipatria Fault.

The herein named Estelle Fault is Meidav's (1970) Fault 15 and similar to the unnamed inferred fault of Lynch and Hudnut (2008) that lies between the Whister and Calipatria faults. North of Mullet Island, Meidav's Fault 15 is exactly coincident with the eastern limit of the magnetic intrusion interpreted by Griscom and Muffler (1971). CTR surveyed three seismic lines over the area where its wells P1-1 and P1-2 are located (Figure 1). The Calapatria and Estelle Faults are clearly indicated by offsets in the uppermost prominent reflector zone and there is a well-developed PRZ between the two faults.

The herein named M17 Fault is an extension of Meidav's (1970) Fault 17. On published shallow thermal gradient maps for the eastern SSGF there are data for five shallow thermal gradient wells that were discarded because they were non-linear (Newmark et al., 1988). One is on the Calipatria Fault, one is on the Whister Fault, and three are located between the Estelle and Whister faults. We interpret this zone of non-linear data to indicate a zone of shallow thermal convection associated with the NW striking M17 Fault.

4.2 NE Striking Regional Faults

The seismically active northeast striking Main Central Fault (Hulen et al., 2003), a.k.a. the Obsidian Butte Fault (Lohman and McGuire, 2007) underlies much of the developed SSGF. The northeast striking Kalin Fault approximately defines the southeast limit of the productive area of the SSGF (Barbour et al., 2016) (Figure 8). Some NE striking faults form sharp contacts between the crystalline basement and the sediment-filled basin (Fuis et al., 1982). Numerous fabric scale Quaternary NE striking faults are present between the southern Salton Sea and the western basin edge (Magistrale et al., 1989; USGS, 2024).

NE striking faults have been interpreted to be seafloor spreading centers like those recognized in the Gulf of California (e.g. Elders et al., 1972; Kaspereit et al., 2016). We interpret that the NE striking faults in the SSGF are not spreading centers (see also Dorsey and Umhoefer, 2012). In support of this interpretation, CTR seismic lines that cross the inferred spreading center of Kaspereit et al. (2016) at Mullet Island have no offset of continuous reflectors where the spreading center is inferred.

The NE striking regional faults are sometimes interpreted as sinistral conjugate R' faults to NW striking dextral faults (Brothers et al., 2009; Kaspereit et al., 2016) implying Reidel shear zone genetic relationship. However, the fault morphologies are not consistent with R' faults as described in literature (Tchalenko, 1970; Davis et al., 2000) and R' faults are rarely significant mineralized permeability structures (e.g. Sims, 1993). Willis and Tosdal (1992) provide an excellent example for permeability distribution in a Reidel shear zone at the Mesquite mine, located on the eastern side of the Salton Trough, and interpreted to be potentially related to early rift development. Mineralization is Oligocene and S_{Hmax} was the same as it is today, but the principal and intermediate stresses are switched relative to our interpreted current SSGF stress field. Essentially all permeability is in R faults and NNE striking tensional structures.

The 1987 Elmore Ranch and Superstition Hills earthquakes are also instructive. The seismic relationship of the NE striking Elmore Ranch and NW striking Superstition Hills faults earthquakes is unique for the United States and observed only in several instances world-wide (Hanks et al., 1989). The NE striking fault earthquakes were deeper than those on the NW striking fault (Magistrale et al., 1989), and the cross-strike extent of surface rupture is significantly greater than the aftershocks that lie beneath them (Hanks et al., 1989).

We interpret that the NE striking regional structures are not genetically related to the NW striking faults. Instead, these are over a deep reactivated arc-perpendicular fault that formed in response to differential compressional movement or irregularities in the overlying crust or the underlying slab during earlier subduction. Examples for arc-perpendicular faults hosting magmatic ore deposits at their intersections with major arc-parallel regional structures are found in Chile (Garrido et al., 2002), New Guinea (Hill et al., 2002), Mexico (Valencia-Moreno et al., 2007), and Yukon/Alaska (Sanchez et al., 2013). Some young Mexican ore deposit locations are controlled by arc-perpendicular faults that hosted porphyry copper deposits during Laramide compression and were reactivated during younger extension (Camprubi and Albinson, 2007). Intersections with young faults that parallel the paleo-arc are favorable locations (Sims, 2008). Sanchez et al. (2013) imaged the internal fault geometry of several arc-perpendicular fault lineaments. The lineaments are tens of kilometers wide and fault geometry within the lineaments is similar with the NE striking faults mapped west of the SSGF.

The arc-perpendicular fault lineament that, at its intersection with the Salton Trough rift, controls the location of the SSGF, is the herein described Jacumba Lineament. It is approximately 30 miles (18.5 km) wide. The northeast corner of the NE striking lineament is at the southern termination of the San Andreas Fault, where it intersects the Brawley Fault. It extends southwest near the Salton Sea hinge zone of Brothers et al. (2009), through a NE striking San Felipe Fault zone segment, and southwest to the Thing Valley Fault (Merifield and Lamar, 1979). The southeastern limit of the Jacumba Lineament is approximately at the Slab City hot springs, extending southwest on unnamed faults north of Coyote Creek, to the NE striking Ocotillo Fault zone, then to Jacumba Hot Springs and the active NE striking fault on the northwest side of Sierra Juarez Mountain in northern Mexico, with at least 300 meters of vertical displacement, down on the northwest (Swenson, 1981).

Aftershocks from the 2010 Seirra El Mayor M 7.2 earthquake extended northwards from Mexico to the intersection with the southern limit of the Jacumba Lineament where they essentially terminated. This is consistent with the characteristic termination of arc parallel faults and folds at intersections with arc-perpendicular lineaments at other locations. Aftershocks were triggered near Jacumba and on the Sierra Juarez Mountain Fault. Flow rates of artesian hot springs at Jacumba increased substantially the day following the earthquake and the water smelled of sulfur (Houser and Murbach, 2014).

Magmatic and hydrothermal features within the Jacumba Lineament include the Salton Buttes and SSGF, the Superstition Mountains geothermal system, the Alverson volcanic field, several hot springs, late Cretaceous volcanic rocks of the Table Mountain Formation, and the overlying 18.7+/- 1.3 ma Jacumba volcanic field (Tamborell, 2015; Byron, 2015). The anomalous Fish Creek Vallecito Basin (Dorsey et al., 2011) and detachment faults (Dorsey and Umhoefer, 2012) are also partially within this lineament (Figure 9).

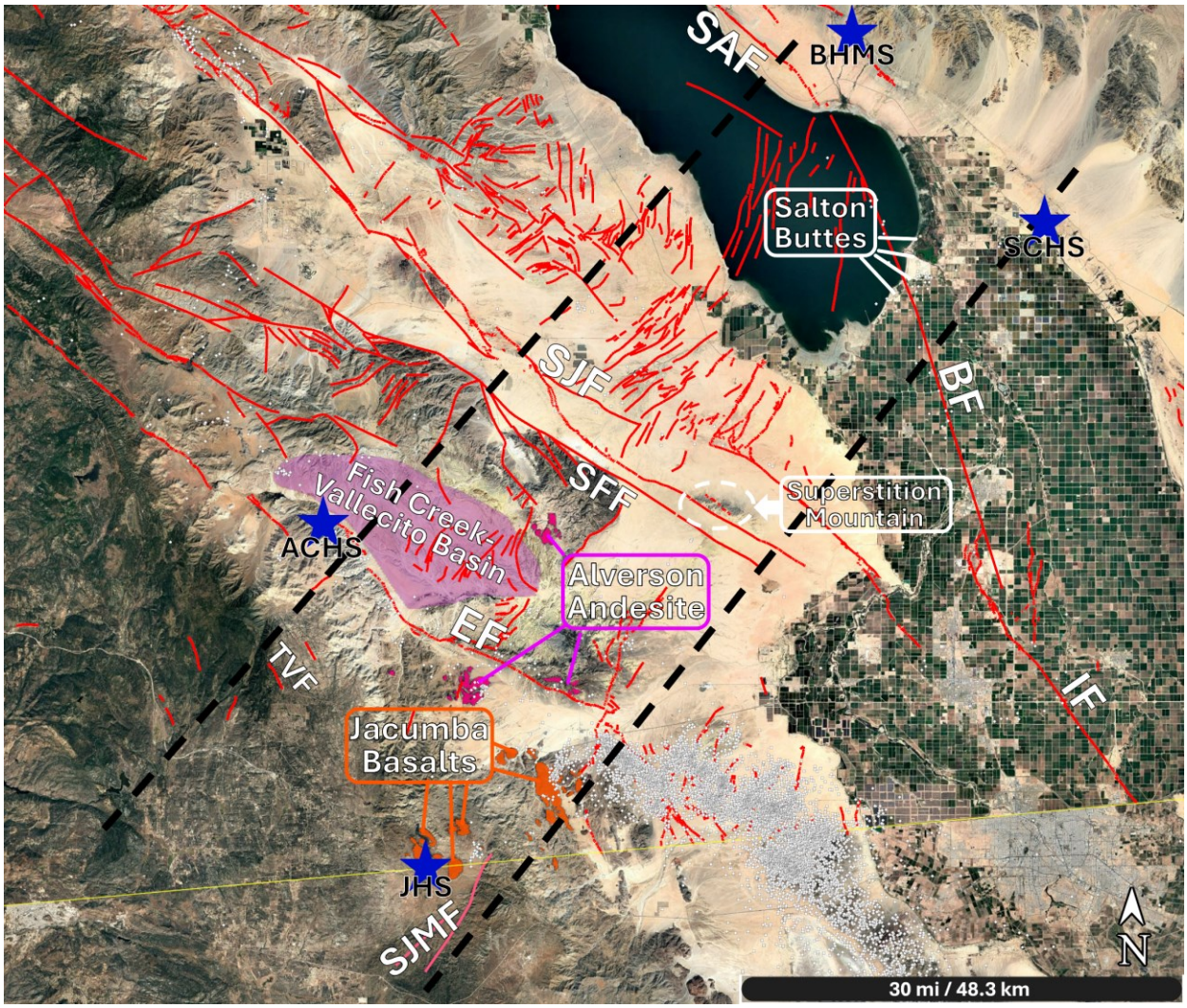

Figure 9: Jacumba Lineament. Red faults (USGS, 2024). The 2010 Seirra El Mayor M 7.2 earthquakes (white dots) have date range: April 1-July 30, 2010 (from USGS, 2025). BHMS - Bashford's Hot Mineral Spa; SCHS - Slab City Hot Springs; ACHS - Agua Caliente Hot Springs; JHS - Jacumba Hot Springs; SAF - San Andreas Fault; BF - Brawley Fault; IF - Imperial Fault; SJF - San Jacinto Fault; SFF - San Felipe Fault; EF - Elsinore Fault; TVF - Thing Valley Fault; SJMF - Sierra Juarez Mountain Fault.

4.3 NNE Striking Regional Faults

NNE striking faults predominate in the shallow seismic survey of the southern Salton Sea (Brothers et al., 2009). The production zone at Heber is centered on the intersection of a NNE striking normal fault and a NW striking strike slip fault with enhanced permeability mostly following the strike and dip directions of the normal fault (James et al., 1987). In CTR wells, most fabric scale structures, including likely production zone structures, strike NNE. Considering the Weibel distribution for length and spacing for structure sets (Nicholas and Sims, 2000) and the lack of fabric scale structures for NW and NE striking sets within the rock mass, the CTR well data are consistent with an interpretation that NNE striking fractures and normal faults are the only structures newly forming throughout the rock mass in the present stress field, as is predicted by Withjack and Jamison (1986) for a divergence angle >30°.

4.4 Brawley Fault Zone

Seismic reflection and other data indicate that the Brawley Fault is young relative to other regional faults in the Salton Trough and may be as young as the formation of the SSGF (Larsen and Reilinger, 1991). The Brawley Fault is the only regional fault that exhibits shear zone peak or post peak stage behavior as described by Tchelanko (1970). Earthquakes define active faults in the R and R' orientations as well as faults in the NNE orientation (Hauksson et al., 2012). The R' faults are closely spaced and the strike lengths for all are similar. The near-uniform strike lengths of these faults do not require barrier faults. Uniform R' fault lengths are characteristic for a Reidel shear zone, centered over a single slip plane at depth (Tchelanko, 1970; Davis et al., 2000). Within such systems, the R structures and the NNE structures striking parallel to S_{Hmax} are the principal permeability structures.

5. FABRIC SCALE STRUCTURE AND HYDROTHERMAL/TECTONIC BRECCIA WITHIN THE PRZ

The PRZ is coincident with but not limited to regional fault damage zones that are expected to rarely exceed a few hundred meters in width (Faulkner et al., 2011; James et al., 1987). We interpret that the ubiquitous reservoir related PRZ at the SSGF results from fabric scale faults and fractures, hydrofractures and hydrothermal breccia within the rock mass. Scientific well State 2-14 is the best-studied well in the SSGF and it provides examples of all these permeability elements. It does not intersect a regional fault but may be within a damage zone (Figure 1), so all structure is fabric scale. Within tens of feet of significant permeability structures, the abundance of euhedral crystals in cuttings can exceed 40%, each crystal up to 0.75 inches long (GeothermEx, 1986a). An example of euhedral crystals in hydrothermal/tectonic breccia from a Hudson Ranch well (Sims, 2013) is presented in Figure 10.

State 2-14 is the only well in the SSGF with significant core footage and breccia was logged through much of the well, with base metal mineralized breccia and veins reported as shallow as 2,450 feet (GeothermEx, 1986a). An example of fluidized breccia from 4,020 feet in well State 2-14 core is provided in Figure 11. The matrix supported fluidized breccia emanates from a sandstone layer and widens upwards. The processes that produce such hydrothermal breccia, related to normal faults but independent of shearing, are well-described by Philips (1972).

We interpret from cuttings, core and seismic reflection data that fluidized breccia occurs at many scales. At the SSGF scale, the dual porosity reservoir is within the Borrego Formation, which is mudstone and siltstone dominated, and the sand content increases substantially in the underlying Palm Springs Formation (Dibblee, 1954; Herzig et al., 1988). The sand rich unit provided a thick sourceregion to produce large, fluidized breccia bodies as the metasomatic system prograded upwards.

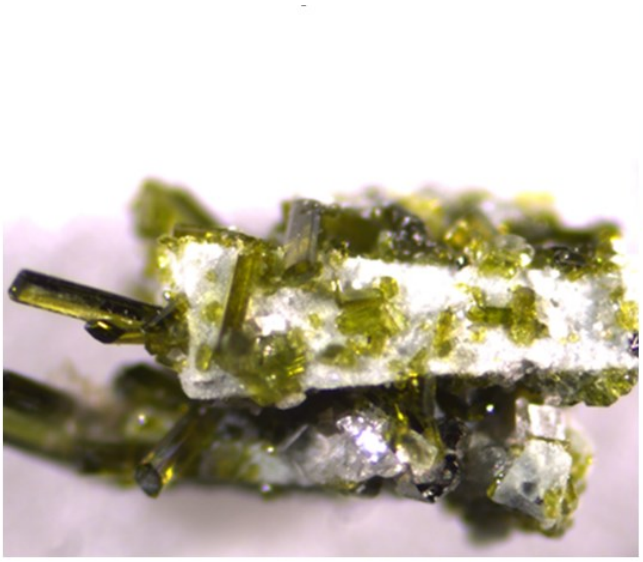

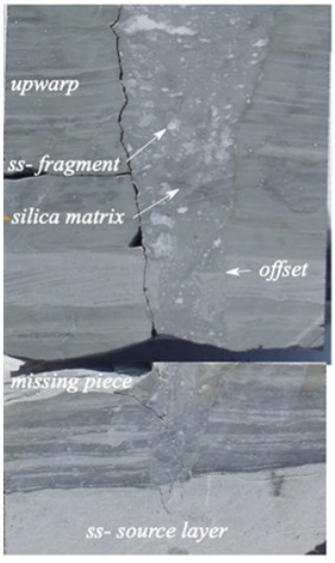

Figures 10 (left) and 11 (right): Left-Hydrothermal/tectonic breccia. White albite crystals and epidote crystals approximately 1mm in length coat breccia fragments (Sims, 2013); Right-Fluidized breccia in siltstone in well State 2-14 core (D.L. Norton) ss= sandstone.

6. RIFT DIVERGENCE, STRESS AND STRAIN

The geometry and evolution of stress, faults, earthquakes, magmatism and fluid flow within the northern Salton Trough are consistent with a regional transtensional-dialational stepover ("TDS") model described by De Paola et al. (2007). A TDS forms between two discontinuous subparallel strike-slip faults. At an angle of oblique divergence less than 30° and low strain rate, wrench-dominated transtension prevails. At greater divergence angles and higher strain rates, extension dominated transtension prevails. A basin may start with wrench dominated transtension and as strain increases switch to extension dominated transtension. The earlier formed strike-slip faults are favorably oriented for reactivation. Withjack and Jamison (1985) further provide that where the divergence angle is greater than 30°, σ_1 is vertical. At a divergence angle greater than 30° strike slip faults no longer form (Withjack and Jamison, 1985; De Paola et al., 2007). Newly formed faults are moderately dipping normal faults that strike oblique to the rift axis. As the oblique angle increases the new normal faults become aligned more parallel to the rift axis.

We interpret a divergence angle greater than 30° in the northern Salton Trough. The direction of divergence is approximately parallel with the San Andreas Fault on the southern edge of the Transverse Ranges and related to the subparallel sinistral faults including the Pinto Mountain Fault Zone and the Blue Cut Fault (USGS, 2024) at the northern extent of the Salton Trough (Figure 12).

The NNE striking normal faults identified by Brothers et al. (2009) at shallow depths and the nearly exclusive NNE striking and moderately dipping structure in the rock mass in CTR well P1-1 to the total true depth of 6,700 feet match the predicted conditions. Brothers et al. (2022) interpret that normal faults have dominated for the last several thousand years. The CTR well data and the presence of the 0.76 Ma Bishop Tuff at 5,600 ft. depth in nearby well State 2-14 indicates this stress configuration, favorable for normal faults, has persisted for at least 0.76 million years. NW and NE striking fabric scale structures are not represented in the rock mass because they cannot form in the extant stress field (Withjack and Jamison, 1985; De Paola et al., 2007). The regional faults in these orientations are reactivated faults that formed in an earlier stress field when the divergence angle was less. Related fault damage and shear in the overlying rock and sediments is limited to the areas immediately above and adjacent to the NE and NW striking reactivated faults.

This complex pattern of tensional fractures, reactivated oblique slip faults, intrusions and veins is commonly known as a Hill-type mesh. The mesh comprises tensile fractures striking parallel to σ_1 that may host dikes, veins and fluid flow, connected by reactivated shear-extensional faults (Hill, 1977; Sibson, 1996; De Paola et al., 2007). Throughgoing linkage faults between the bounding strike slip faults have a staircase trajectory, following the shear and tensile structures. In a right lateral fault system, the linkage fault trajectory is right stepping (De Paola et al., 2007).

The youthful Brawley Fault is thus predicted by the model. It is a linkage structure between the Imperial and San Andreas Faults. Where the fault steps over on NE striking structures, the step is right, and not left, as would be predicted by interpreted sinistral movement on these faults. The fault zone is experiencing peak to post peak stage deformation (Tchelanko, 1970) above a discrete narrow fault at depth because of its youthful age. Eventually, the fault will reach the residual stage, and it will be a thoroughgoing PDZ structure bounding the North American and Pacific plates.

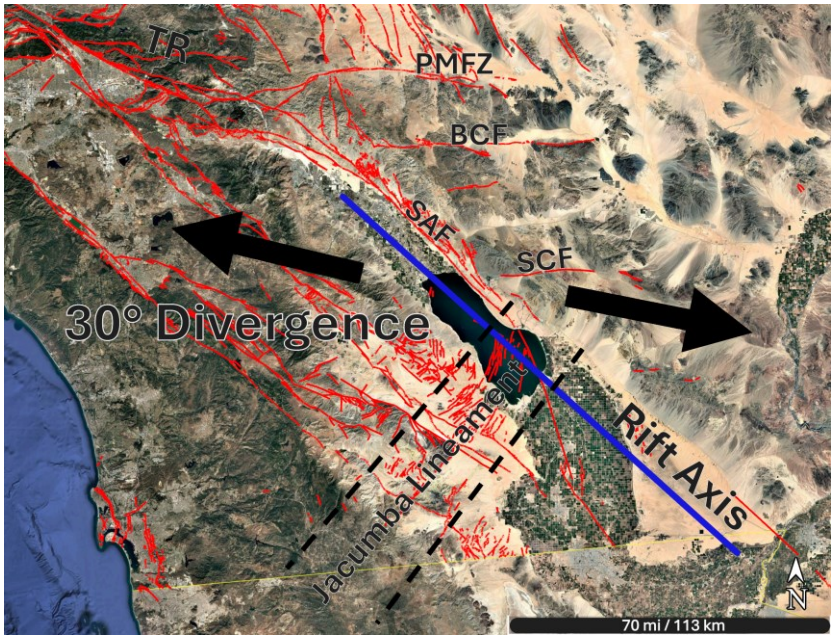

Figure 12: Rift Divergence. The Blue line is the rift axis. Black arrows indicate a divergence angle of 30° (counterclockwise). Red lines are Quaternary faults (USGS, 2024). SAF - San Andreas Fault; PMFZ – Pinto Mountain Fault Zone; BCF – Blue Cut Fault; SCF-Salt Creek Fault; TR- Transverse Ranges.

7. PERMEABILITY MODEL IN THE DUAL POROSITY RESERVOIR

We compiled data to inform modelled permeability for regional faults, and the rock mass within the dual porosity reservoir (approximate depth interval of 1-3 km, includes fracture and fault porosity and intrinsic sediment porosity). Helgeson (1968) and field observations provide that permeability in the SSGF is provided mostly by faults and fractures and this should be followed in models. The reactivated NW and NE striking faults provide horizontal and near vertical permeability enhanced at regional fault intersections and favorable bends in strike. The rock mass hosts NNE striking tensional fractures and normal faults that provide horizontal and vertical permeability.

Enhanced strike-parallel horizontal permeability of normal faults is expected where the rock competency abruptly increases (Sibson, 2000). Shear is expected in the low competency rock and dilation in the high competency rock (Sibson, 1996; Ferrill and Morris, 2001). This is observed near the bottoms of both CTR wells where significant mud losses occurred at the contact with relatively competent sand intervals and continued through the sand intervals. It is an important distinction that the mud losses are attributed to structural permeability in normal faults and fractures and not formation permeability in the competent indurated and metasomatized sand units. Pervasively fractured rock is also observed throughout the eastern portion of the SSGF at a depth of approximately 2 km (Grogan, 1987), where there is a rapid decline in the velocity gradient (Han, 2016), likely attributed to an increase in rock competency. The interaction of normal faults and tensional fractures form a 3D permeability mesh in the rock mass.

Estimated rock mass permeability and fracture spacing for CTR wells are presented earlier in this paper. Rocha et al. (2024) reported permeability values as high as 6,000 md in discrete flow zones at neighboring Hudson Ranch. Morse and Stone (1979) reported a multiple-well "reservoir permeability" in the central SSGF of 250 to 1,000 md, and we believe this includes contributions from rock mass fabric and regional structure.

In well State 2-14, the first flow test was performed with the well drilled to 6,227 feet (Geothermex 1986b, Ross, 1992). There was a 50-foot mud loss zone intercepted before drilling was stopped and a flow test was performed. This loss was in a fabric scale structure likely within the Estelle Fault damage zone. GeothermEx (1986b) reported a permeability of 60 md or 230 md (it is not provided whether the 50-foot loss zone or the entire open hole was used in calculating permeability). With continued drilling, at about 200 feet below the bottom hole depth during the flow test, the well intersected a total loss zone 200 feet in measured length, within presumed fabric-scale structure. Even though the well is vertical, and mineralized structures have steep dips (Caruso et al., 1988), so the structures are largely within the well's blind zone, between 6,000 and 10,564 feet, nine major loss zones were encountered (Ross, 1992).

Reported permeability for Heber is similar. James et al. (1987) and Hoang et al. (1987) apply 2,000-foot vertical intervals and regional faults have Kh values ranging from 100,000 to greater than 200,000 md-ft. Rock mass permeability between 2,000 and 4,000 feet is 50,000 to 150,000 md-ft., enhanced near faults. Rock mass permeability at the base of the dual porosity reservoir between 8,000 and 10,000 feet is 10,000 md-ft. Structural permeability far exceeds formation permeability at reservoir depth (Hoang et al., 1987).

8. MAGMA, STRUCTURE, PERMEABILITY AND POROSITY BELOW THE DUAL POROSITY RESERVOIR

USGS Circular 790 recommended that the maximum depth for assessment of geothermal reservoirs was 3 km (Williams et al., 2008), which is the maximum depth for published reservoir models for the SSGF (e.g. Araya and O'Sullivan, 2022; Dobson et al., 2023). But that recommendation has been superseded to extend to the depth of the brittle-ductile transition, or 6 km maximum, where, as is the case at the SSGF, the base of the system is not drill tested (Williams et al., 2008). Earthquakes are good evidence for the depth of the brittle zone, and they extend to approximately 10 km. Han (2016) used seismic velocity to interpret normal faults to 10 km depth and a kilometers long and wide magmatic igneous body beneath that. Smaller isolated intrusions have been discovered within drilled depths in geothermal fields throughout the Salton Trough (Browne, 1977; Sternfeld and Sternfeld, 1982; Experiments Panel, 1983; Herzig et al., 1988; Schmidt and Hulen, 2008).

SSGF intrusions at all scales are episodic and each intrusion produces a thermal pulse and attendant fluid pressure increase. Substantial porosity and permeability are created in the host rock owing to physical and chemical processes of magmatic intrusion (Norton and Knight, 1977; Knapp and Knight, 1977; Norton, 1984, 1988, and 1990; Dutrow and Norton, 1995). Magmatic ore deposits, which are well-exposed in outcrops and in mines, are used as examples for understanding processes in active geothermal systems (White, 1981; Sasada, 2000). Eldursi et al. (2009) reported that fractured thermal caps persist above ore-related intrusions that extend laterally for kilometers, with fractured caps extending up to 3 km height above the intrusions. Altered or mineralized fracture density at the Sierrita porphyry deposit ranges from approximately 15 mineralized fractures per meter at the center to 3 per meter at 3 km from the center (Haynes and Titley, 1980). Total alteration mineral abundance in and adjacent to veins in porphyry copper systems, and therefore maximum possible instantaneous porosity, is 10% (Titley, 1990).

The upward migrating intrusions are hosted by regional faults that necessarily persist to depths greater than the intrusions that they host. Example data for permeability and porosity of a mineralized fault within an igneous intrusion are provided by Villas and Norton (1977). Measured fractures/meter range from 6-21, with the highest values closest to the fault. Porosity within the fault zone is mostly 1-4% with isolated zones < 1% and > 4%.

The rock mass fabric structure characteristics between the top of the magma breccia cap and the base of the dual porosity reservoir are not sampled by drilling but they are partially sampled for the relatively short time that earthquake data have been collected. All three structure sets and the structures of the Brawley Fault Zone are represented. The apparent relationship of earthquakes triggered by injectate requires fabric scale structural permeability connecting the dual porosity reservoir to the underlying rock. Also, Baker Hughes'

reservoir model for CTR required substantial brine upflow to achieve a reasonable match to the native state. With the available data, it is reasonable to model brine that is transported vertically between the breccia cap and the dual porosity reservoir on regional and fabric scale structures.

Heat flow at the near surface throughout the SSGF area (560 km^2), underlain by regions of rock mass fabric and regional structure, is greater than 200 mW/m^2 (Goldstein and Flexser, 1984; Lachenbruch et al., 1985). Heat flow determined from shallow thermal gradient data in the center SSGF exceeds 500 mW/m^2 and in the Mullet Island and Kornbloom Road areas, the heat flow exceeds 1,200 mW/m^2 (Newmark et al., 1988). Modelled heat flux into the system from below 3 km depth must be at least as great as natural outflow.

9. CONCLUSION

Significant structural permeability exists throughout the rock mass of the dual porosity reservoir. Regional fault and fabric scale structural permeability persists through the base of the dual porosity reservoir and models should allow upflow of brine and downflow of dense injectate through the 3 km barrier at all scales. Without allowing injected brine to drop at injection well sites through rock mass permeability, potential induced earthquakes, flow paths and production depletion rates will be poorly modelled. Necessary modelling of the sub 3 km depth magma-hydrothermal system will require an appropriate Equation of State (e.g. Brikowski et al., 2001) and additional work.

The dual porosity reservoir rock mass permeability values presented here are at least an order of magnitude greater than values reported by Araya and O'Sullivan (2022). Their model assumes that vertical permeability is very limited to regional "upflow faults" and that vertical permeability in the rock mass at dual porosity reservoir depths ranges between 0.1 and 0.5 md, and horizontal permeability exceeds vertical permeability. The depth of their model is software limited to a maximum temperature of 360° C (O'Sullivan et al., 2024) which is the 3 km floor. These data were applied to assess a reinjection plan that reduces chemical breakthrough and Li depletion (O'Sullivan et al., 2024).

After this work, Schill et al. (2025) provided that "effective reservoir management will require more than just conceptual strategies—it will require more precise, detailed reservoir models that incorporate and account for the inherent uncertainties in model forecasts." Supporting this effort, CTR presents the data and recommendations contained herein. Applying these data, the sensitivity analysis of Barton et al. (2025) demonstrates that, with a 3 km floor, an increase in base case rock mass permeability by 5x can significantly decrease model Li depletion rates at production wells. We believe that removing the 3 km floor will further decrease model Li depletion rates and that the recommended work is necessary prior to further assessment of SSGF field development plans.

REFERENCES

Araya, N. and O'Sullivan, J.: A 3D conceptual and natural-state model of the Salton Sea Geothermal Field. Geothermal Resources Council Transactions, 46, (2022), 2153-2159.

Barbour, A.J., Evans, E.L., Hickman, S.H., and Eneva, M.: Subsidence rates at the southern Salton Sea consistent with reservoir depletion. Journal of Geophysical Research, 121, (2016), 5308-5327.

Barton, C., Pettit, W., Salter, T., Meyer, E., Harper, C., Nasir, E., Moradi, A., Sims, D., and Osborn, W.: Next generation reservoir modeling for geothermal energy and lithium recovery. Proceedings, 50th Workshop on Geothermal Reservoir Engineering, Stanford University, Stanford, California, (2025).

Blakeslee, S.: Seismic discrimination of a geothermal field: Cerro Prieto. GRC Transactions, 8, (1984), 183-188.

Brikowski, T., Norton, D.L., and Blackwell, D.: Final report: Natural state models of The Geysers geothermal system. DOE Contract DE-FG07-98ID13677, (2001), 75 p.

Brothers, D.S., Driscoll, N.W., Kent, G.M., Baskin, R.L., Harding, A.J., and Kell, A.M.: Seismostratigraphic analysis of Lake Cahuilla sedimentation cycles and fault displacement history beneath the Salton Sea, California, USA. Geosphere, 18, (2022), 1354–1376.

Brothers, D.S., Driscoll, N.W., Kent, G.M., Harding, A.J., Babcock, J.M., and Baskin, R.L.: Tectonic evolution of the Salton Sea inferred from seismic reflection data. Nature Geoscience, 2, (2009), 581-584.

Browne, P.R.L.: Occurrence and hydrothermal alteration of diabase, Heber Geothermal Field, Imperial Valley, California. University of California Riverside, Institute of Geophysics and Planetary Physics, Paper 77/9, Riverside, CA, (1977), 61 p.

Byron, K.: Geochemical analysis of the Alverson Formation Volcanics in Painted Gorge, Coyote Mountains, Imperial County, California. Unpublished B.S. thesis, San Diego State University, San Diego California, (2015), 28p.

CalGEM: Well-finder, California Department of Conservation, https://maps.conservation.ca.gov/doggr/wellfinder/, (2025).

Call, R.D., Savely, J.P., and Nicholas, D.E.: Estimation of joint set characteristics from surface mapping data. The 17th US Symposium on Rock Mechanics, American Rock Mechanics Association, (1976), 2 B2-1-9.

Camprubi, A., and Albinson, T.: Epithermal deposits in Mexico – update of current knowledge, and an empirical reclassification. *In,* Alaniz-Alvarez, S.A., and Nieto-Samaniego, A.F., (eds.), Geology of Mexico: Celebrating the Centenary of the Geological Society of Mexico: Geol. Soc. of America Special Paper 422, (2007), 377-415.

Caruso, L.J., Bird, D.K., Cho, M., and Liou, J.G.: Epidote-bearing veins in the State 2-14 drill hole: Implications for hydrothermal fluid composition. Journal of Geophysical Research, 93, (1988), 12123-12133.

Celwik, S., Ryan, T.M., and Cicchini, P.F.: Error quantification in oriented-core data and its influence on rock slope design. Slope Stability 2011: International Symposium on Rock Slope Stability in Open Pit Mining and Civil Engineering, Vancouver, Canada, (2011).

Cho, M., Liou, J.G., and Bird, D.K.: Prograde phase relations in the State 2-14 well metasandstones, Salton Sea Geothermal Field, California. Journal of Geophysical Research, 93, (1988), 13081-13103.

Chou, C.-K.: A study of phyllosilicates from the Fee #5 well, Salton Sea Geothermal Field, California, USA. Unpublished M.Sc..thesis, University of California Riverside, Riverside California, (1989), 90 p.

Crandall-Bear, A., Barbour, A.J., and Schoenball, M.: Irregular focal mechanisms observed at Salton Sea Geothermal Field: Possible influences of anthropogenic stress perturbations. Proceedings, 43rd Workshop on Geothermal Reservoir Engineering, Stanford University, Stanford, CA (2018).

Davis, G,H., Bump, A.P., Garcia, P.E., and Ahlgren, S.G.: Conjugate Reidel deformation band shear zones. Journal of Structural Geology, 22, (2000), 169-190.

De Paola, N., Holdsworth, R.E., Collettini, C., McCaffrey, K.J.W., and Barchi, M.R.: The structural evolution of dilational stepovers in regional transtensional zones. *In*, Cunningham, W. D. & Mann, P., (eds), Tectonics of Strike-Slip Restraining and Releasing Bends, Geological Society of London Special Publication 290, (2007), 433–445.

Dibblee, T.W., Jr.: Geology of the Imperial Valley region, California. *In* Jahns, R.H., (ed.), Geology of Southern California: California Department of Natural Resources, Division of Mines Bulletin 170, (1954), 21–28.

Dobson, P., Araya, N., Brounce, M., Busse, M., et al.: Characterizing the Geothermal Lithium Resource at the Salton Sea. Technical Report to the U.S. Department of Energy Geothermal Technologies Office, (2023).

Dorsey, R.J., Housen, B.A., Janecke, S.U., Fanning, C.M., and Spears, A.L.F.: Stratigraphic record of basin development within the San Andreas fault system: Late Cenozoic Fish Creek-Vallecito basin, southern California. Geological Society of America Bulletin, 123 (5–6), (2011), 771–793.

Dorsey, R.J., and Umhoefer, J.J.: Influence of sediment input and plate-motion obliquity on basin development along an active oblique-divergent plate boundary: Gulf of California and Salton Trough. *In,* Busby, C. and Azor, A., (eds.), Tectonics of Sedimentary Basins: Recent Advances, First Edition, Chichester, West Sussex, UK, Hoboken, NJ, Wiley-Blackwell (2012).

Dutrow, B., and Norton, D.L.: Evolution of fluid pressure and fracture propagation during contact metamorphism. Journal of Metamorphic Geology, 13, (1995), 677-686.

Elders, W.A., Rex, R.W., Meidav, T., Robinson, P.T., and Biehler, S.: Crustal spreading in southern California, the Imperial Valley and Gulf of California formed by the rifting apart of a continental plate. Science, 178, (1972), 15-24.

Eldursi, K., Branquet, Y., Guillou-Frottier, L., and Marcoux, E.: Numerical investigation of transient hydrothermal processes around heat intrusions: heat-transfer and fluid-circulation controlled mineralization patterns. Earth and Planetary Science Letters, 288, (2009), 70-83.

Evans, J.P., Forster, C.B., and Goddard, J.V.: Permeability of fault-related rocks, and implications for hydraulic structure of fault zones. Journal of Structural Geology, 19, (1997), 1393-1404.

Experiments Panel: Proposed scientific activities for the Salton Sea scientific drilling project. Institute of Geophysics and Planetary Physics, University of California, Riverside, (1983), 132 p.

Faulkner, D.R., Mitchell, T.M., Jensen, E., and Cembrano, J.: Scaling of fault damage zones with displacement and the implications for fault growth processes. Journal of Geophysical Research., 116, (2011), B05403.

Ferrill, D.A. and Morris, A.P.: Dilational normal faults. Report to the US Nuclear Regulatory Commission, July 3, (2001), 12 p.

Fitch, M.K.: History of development of the Salton Sea area. Unpublished M.A. thesis, University of Southern California, Los Angeles, CA, (1961), 296 p.

Fuis, G.S., and Kohler, W.M.: Crustal structure and tectonics of the Imperial Valley region, California. *In,* Rigby, C.A., (ed.), The Imperial Basin - tectonics, sedimentation and thermal aspects. Society of Economic Paleontologists and Mineralogists, Pacific Section Publication, (1984), 1-13.

Fuis, G.S., Mooney, W.D., Healey, J.H., McMechan, G.A., and Lutter, W.M.: Crustal structure of the Imperial Valley region. *In*, The Imperial Valley California, Earthquake of October 15, 1979, U.S. Geological Survey Prof. Paper 1254, (1982), 25 p.

Garrido, I., Cembrano, J., Siña, A., Stedman, P., and Yañez, G.: High magma oxidation state and bulk crustal shortening: key factors in the genesis of Andean porphyry copper deposits, central Chile (31-34°S)'. Revista Geológica de Chile, 29, (2002), 43-54.

GeothermEx, Inc.: Well-test report Hell's Kitchen (HK-1 and HK-2) Salton Sea, California. Prepared for Controlled Thermal Resources Inc., proprietary, (2022), 70p.

GeothermEx, Inc.: Salton Sea Scientific Drilling Program, Geologic Interpretation of Well State 2-14. Prepared for Bechtel National, Inc., three appendices including descriptive logs for cuttings and core, (1986a).

GeothermEx, Inc.: Salton Sea Scientific Drilling Program, Flow Test of Well State 2-14, 28-30 December 1985. Prepared for Bechtel National, Inc., (1986b).

Goldstein, N.E., and Flexser, S.: Melt zones beneath five volcanic complexes in California – an assessment of shallow magma occurrences. Lawrence Berkley Laboratory, University of California, LBL-18232, (1984), 134 p.

Griscom, A., and Muffler, L.J.P.: Aeromagnetic map and interpretation of the Salton Sea geothermal area, California. USGS Geophysical Investigations Map GP-754, (1971).

Grogan, L.L.: Compilation of well Wilson 1-12 data and proprietary technical reports submitted to the California State Lands Commission supporting Kennecott Minerals application for a state geothermal lease, (1987).

Han, L.: Seismic imaging and thermal modeling of active continental rifting processes in the Salton Trough, southern California. Unpublished Ph.D. thesis, Virginia Polytechnic Institute and State University, Blacksburg, VA, (2016), 137 p.

Hanks, T.C., and Allen, C.R.: The Elmore Ranch and Superstition Hills earthquakes of 24 November 1987: Introduction to the special issue. Bulletin of the Seismological Society of America, 79, (1989), 231–238.

Hauksson, E., Yang, W., and Shearer P.M.: Waveform relocated earthquake catalog for Southern California (1981 to 2011). Bulletin Seismological Society of America, 102, (2012) and updated catalogs at https://scedc.caltech.edu/data/alt-2011-yang-hauksson-shearer.html.

Haynes, F.M., and Titley, S.R.: The evolution of fracture-related permeability within the Ruby Star granodiorite, Sierrita porphyry copper deposit, Pima County, Arizona. Economic Geology, 75, (1980), 673-683.

Helgeson, H.C.: Geologic and thermodynamic characteristics of the Salton Sea geothermal system. American Journal of Science, 266, (1968), 129-166.

Herzig, C.T., Mehegan, J.M., and Stelting, C.E.: Lithostratigraphy of the State 2-14 borehole, Salton Sea Scientific Drilling Project. Journal of Geophysical Research, 93, (1988), 12,696-12,980.

Hill, D.P.: A model for earthquake swarms. Journal of Geophysical Research, 82, (1977), 1347-1352.

Hill, K.C., Kendrick, D.D., Crowhurst, P.V., and Gow, P.A.: Copper-gold mineralization in New Guinea: tectonics, lineaments, thermochronology and structure. Australian Journal of Earth Sciences, 49, (2002), 737-752.

Hoang, V.T., James, E.D., and Epperson, I.J.: Heber Geothermal Field: Reservoir and Production Characteristics. Society of Petroleum Engineers, SPE 16339, (1987), 151-158.

Holt, R.: Well test analysis: HK-1 and HK-2 flow tests March and April 2022, draft. Prepared for CTR, proprietary, (2022).

Houser, C.E., and Murbach, M.L.: High desert lore and hydrogeology of the Jacumba Valley, Jacumba Hot Springs, San Diego County, California. *In*, Coast to Cactus, Geology and Tectonics, San Diego to Salton Trough, California, SDAG 2014 Field Trip Guidebook, (2014), 99-108.

Howard, J.H., Apps, J.A., Benson, S.M., Goldstein, N.E., Graf, A.N., Haney, J.P., Jackson, D.D., Jusprasert, S., Majer, E.L., McEdwards, D.G., McEvilly, T.V., Narasimhan, T.N., Schechter, B., Schroeder, R.C., Taylor, R.W., van de Kamp, P.C., and Wolery, T.J.: Geothermal resource and reservoir investigations of U.S. Bureau of Reclamation leaseholds at East Mesa, Imperial Valley, California. Lawrence Berkley Laboratory, (1978), 243 p., 6 appendices.

Hulen, J.B., Kaspereit, D., Norton, D.L., Osborn, W., and Pulka, F.S.: Refined conceptual modeling and a new resource estimate for the Salton Sea Geothermal Field, Imperial Valley, California. Geothermal Resources Council, Transactions, 26, (2002), 29-36.

Hulen, J.B., Norton, D.L., Moore, J.N., Osborn, W., van de Putte, T., and Kaspereit, D.: The role of sudden dilational fracturing in evolution and mineralization of the southwestern Salton Sea geothermal system, Imperial Valley California, Proceedings, 28th Workshop on Geothermal Reservoir Engineering, Stanford University, Stanford, CA (2003).

James, E.D., Hoang, V.T., and Epperson, I.J.: Structure, permeability and production characteristics of the Heber, California geothermal field. Proceedings, 12th Workshop on Geothermal Reservoir Engineering, Stanford University, Stanford, CA (1987).

Kaspereit, D., Mann, M., Sanyal, S., Rickard, W., Osborn, W., and Hulen, J.: Updated conceptual model and resource estimate for the Salton Sea Field, Imperial Valley, California. Geothermal Resources Council Transactions, 40, (2016), 57-66.

Kelley, V. C., and Soske, J. L.: Origin of the Salton volcanic domes, Salton Sea, California. Journal of Geology, 44, (1936), 496-509.

Knapp, R.B., and Knight, J.E.: Differential thermal expansion of pore fluids—fracture propagation and microearthquake production in hot pluton environments. Journal of Geophysical Research, 82, (1977), 2515-2522.

Lachenbruch, A.H., Sass, J.H., Galanis Jr., S.P.: Heat flow in southernmost California and the origin of the Salton Trough. Journal of Geophysical Research, 90, (1985), 6709-6736.

Larsen, S., and Reilinger, R.: Age constraints for the present fault configuration in the Imperial Valley, California: evidence for northwestward propagation of the Gulf of California rift system. Journal of Geophysical Research, 96, (1991), 10339-10,346.

Lohman, R.B., and McGuire, J.J.: Earthquake swarms driven by aseismic creep in the Salton Trough, California. Journal of Geophysical Research, 112, (2007), B04405.

Lynch, D.K., and Hudnut, K.W.: The Wister mud pot lineament: southwest extension or abandoned strand of the San Andreas Fault?. Bulletin of the Seismological Society of America, 8, (2008), 1720-1729.

Magistrale, H., Jones, L., and Kanamori, H.: The Superstition Hills, California, earthquakes of 24 November 1987. Bulletin of the Seismological Society of America, 79, (1989), 239–251.

McDowell, S.D.: Geothermal alteration of sediments in the Salton Sea scientific drillhole: Petrophysical changes and mass changes during alteration. U.S. Department of Energy Final Research Report 13409-1, (1987), 66 p.

Meidav, T.: Geophysical survey of the southern Salton Sea. *In*, Geothermal wastes and the water resources of the Salton Sea area, California Department of Water Resources Bulletin n. 143-7, Appendix G, (1970).

Merifield, P.M., and Lamar, D.L.: Faults and lineaments in the basement terrane of south-central San Diego County, California. *In,* Abbott, P.L., and Elliott, W.J., (eds), Earthquakes and other perils San Diego region, GSA fieldtrip guide by San Diego Association of Geologists, (1979), 1-10.

Morse, J.G., and Stone, R.: Evaluation of reservoir properties in a portion of the Salton Sea Geothermal Field. Lawerence Livermore National Laboratory, UCRL-52756, (1979), 52 p.

Muffler, J.L.P., and White, D.E.: Active metamorphism of Upper Cenozoic sediments in the Salton Sea Geothermal Field and the Salton Trough, southeastern California. Geological Society of America Bulletin, 80, (1969), 157-182.

Muramoto, F.S., and Elders, W.A.: Correlation of wireline log characteristics with hydrothermal alteration and other properties of the Salton Sea and Westmoreland geothermal systems, Imperial Valley, California, USA. Los Alamos National Laboratory Report LA-10128-MS, (1984), 113 p.

Newmark, R.L., Kasameyer, P.W., and Younker, L.W.: Shallow drilling in the Salton Sea region: the thermal anomaly. Journal of Geophysical Research, 93, (1988), 13,005-13,023.

Nielson, D.L., and Moore, J.N.: Review of the Niland Geothermal Project. Memorandum report from the University of Utah Research Institute, November 14, (1984), 7p.

Nicholas, D.E. and Sims, D.B.: Collecting and using structure data for slope design. *In*, Hustrulid, W.A., McCarter, M.H. and Van Zyl, D.J.A., (eds.), Slope stability in surface mining, SME, Littleton, CO., (2000), 11-26.

Norton, D.L.: Theory of hydrothermal systems. Annual Review of Earth and Planetary Sciences, 12, (1984), 155-177.

Norton, D.L.: Metasomatism and permeability. American Journal of Science, 288, (1988), 604-619.

Norton, D.L.: Pore fluid pressure near magma chambers. *In*, The role of fluids in crustal processes, The National Academies Press, Washington, DC, (1990), 42-49.

Norton, D.L., and Knight, J.: Transport phenomena in hydrothermal systems: cooling plutons. American Journal of Science, 277, (1977), 937-981.

O'Sullivan, J., Araya, N., Popineau, J., Renaud, T., Riffault, J., and O'Sullivan, M.: Investigating reinjection strategies to optimize lithium production from the Salton Sea geothermal field. Proceedings, 49th Workshop on Geothermal Reservoir Engineering, Stanford University, Stanford, CA (2024).

Philips, W.J.: Hydraulic fracturing and mineralization. Journal Geological Society of London, 128, (1972), 337-359.

Rocha, S., Bourdeau-Hernikl, J., Faulder, D.D., and Minguez, D.: Conceptual hydrothermal model of the Salton Sea KGRA, Geothermal Resources Council Transactions, 48, (2024), 22p.

Ross, H.P.: Salton Sea Scientific Drilling Project, a summary of drilling and engineering activities and scientific results, Final Report. DOE/CE-12429-H1, (1992), 186 p.

Sahakian, V., Kell, A., Harding, A., Driscoll, N., and Kent, G.: Geophysical evidence for a San Andreas subparallel transtensional fault along the northeastern shore of the Salton Sea. Bulletin of the Seismological Society of America, 106, (2016), 1963-1978.

Sanchez, M.G., Murray, M.A., Hart, C.J.R, and Mortenson, J.K.: Orogen-perpendicular magnetic segmentation of the western Yukon and eastern Alaska cordilleran hinterland: Implications for structural control of mineralization. Yukon Exploration and Geology 2012, Yukon Geological Survey, (2012),133-146.

Sasada, M.: Igneous-related active geothermal system versus porphyry copper hydrothermal system. Proceedings, World Geothermal Congress, Kyushu-Tohoku, Japan, (2000), 1691-1693.

Schill, E., Busse, M.M., Stringfellow, W.T., O'Sullivan, J., Slattery, M., Nico, P., McKibben, M.A., Brounce, M., and Dobson, P.: The Lithium Valley Project. Proceedings, 50th Workshop on Geothermal Reservoir Engineering, Stanford University, Stanford, California, (2025).

Schmidt, A.K., and Hulen, J.B.: Buried rhyolites within the active, high temperature Salton Sea geothermal system. Journal of Volcanology and Geothermal Research, 178, (2008), 708-718.

Sibson, R.H.: Structural permeability of fluid-driven fault-fracture meshes. Journal of Structural Geology, 18, (1996), 1031-1042.

Sibson, R.H.: Fluid involvement in normal faulting. Journal of Geodynamics, 29, (2000), 469-499.

Sims, D.B.: Geology of the Ash Peak mine, Greenlee County, Arizona. Unpublished M.Sc. thesis, University of Arizona, Tucson, AZ, (1993), 49 p.

Sims, D.B.: Structural geology and ore controls, Guazapares mining district, Chihuahua, Mexico, proprietary, (2008).

Sims, D.B.: Geology at Hudson Ranch: the Salton Sea Geothermal Field. California State University, San Marcos, October 10, (2013).

Sims, D.B.: Use of borehole data in defining structure sets for rock slope kinematic analysis. American Association of Environmental and Engineering Geologists, Program with Abstracts, Colorado Springs, CO, September 15, (2017).

Sternfeld, M.K., and Sternfeld, J.: Hydrothermal alteration and tectonic setting of intrusive rocks from east Brawley, Imperial Valley: an application of petrology to geothermal reservoir analysis. Proceedings, 8th Workshop on Geothermal Reservoir Engineering, Stanford University, Stanford, CA (1982).

Swenson, G.A.: The ground water hydrology of Jacumba Valley, California and Baja California. Unpublished M.Sc. thesis, San Diego State University, San Diego, CA, (1981), 289 p.

Tamborell, D. J.: Petrography and whole rock geochemistry of Tertiary volcanic rock along the eastern flank of the Laguna Juarez, Baja California, Mexico and comparison with the nearby Jacumba Volcanics and Alverson Formation of San Diego and Imperial Counties. Unpublished B.S. thesis, San Diego State University, San Diego, CA, (2015), 23p.

Tchalenko, J.: Similarities between shear zones of different magnitudes. Geological Society of America Bulletin 81, (1970), 1625-1639.

Terzaghi, R.D.: Sources of error in joint surveys. Géotechnique, 15, (1965), 287–304.

Tewhey, J.D.: Geologic characteristics of a portion of the Salton Sea Geothermal Field. Geothermal Resource Council Transactions, 1, (1977), 827-848.

Titley, S.R.: Evolution and style of fracture permeability in intrusion-centered hydrothermal systems, *In*, The role of fluids in crustal processes, The National Academies Press, Washington, DC, (1990), p. 50-63.

USGS: Calipatria CA quadrangle map, 1:62,500 scale, 15 Minute Series Topographic Sheet, (1944).

USGS: Niland CA quadrangle map, 1:24,000 scale, 7.5 Minute Series Topographic Sheet, (1956).

USGS: Quaternary fault and fold database of the United States, (2024). https://www.usgs.gov/programs/earthquake-hazards/faults

USGS: Earthquake catalog for Google Earth, (2025). https://earthquake.usgs.gov/earthquakes/search/

Valencia-Moreno, M., Ochoa-Landin, L., Noguez-Alcantara, B., Ruiz, J., and Perez-Segura, E.: Geological and metallogenetic characteristics of the porphyry copper deposits of Mexico and their situation in world context. *In* Alaniz-Alvarez, S.A., and Nieto-Samaniego, A.F., (eds.), Geology of Mexico: Celebrating the Centenary of the Geological Society of Mexico. Geol. Soc. of America Special Paper 422, (2007), 433-458.

Villas, R.N. and Norton, D.L.: Irreversible mass transfer between circulating hydrothermal fluids and the Mayflower Stock. Economic Geology, 72, (1977), 1471-1504.

White, D.E.: Active geothermal systems and hydrothermal ore deposits. Economic Geology, 75th Anniversary Volume, (1981), 392-423.

Williams, A.E.: Fluid density distribution in a high temperature, stratified thermohaline system: implications for saline hydrothermal circulation. Earth and Planetary Science Letters, 146, (1997), 121-136.

Williams, C.F., Reed, M.J., and Mariner, R.H.: A review of methods applied by the U.S. Geological Survey in the assessment of identified geothermal resources. USGS Open-File Report 2008-1296, (2008), 27p.

Willis, G.F., and Tosdal, R.M.: Formation of gold veins and breccias during dextral strike slip faulting in the Mesquite mining district, south-eastern California. Economic Geology, 87, (1992), 2002-2022.

Withjack, M.O., and Jamison, W.R.: Deformation produced by oblique rifting. Tectonophysics, 126, (1986), 99–124.